Journal of Engineering for Gas Turbines and Power

Copy of e-mail Notification

Journal of Engineering for Gas Turbines and Power Published by ASME

Dear Author,

Congratulations on having your paper accepted for publication in the ASME Journal Program.

Your page proof is available from the ASME Proof site here:

http://115.111.50.156/jw/AuthorProofLogin.aspx?pwd=7ad93504c30a&CA=AS

Login: your e-mail address

Password: 7ad93504c30a

Please keep this email in case you need to refer back to it in the future.

Responsibility of detecting errors rests with the author. Please review the page proofs carefully and:

1. Answer any queries on the “Author Query Form”
2. Proofread any tables and equations carefully
3. Check to see that any special characters have translated correctly
4. Publication will not proceed until a response is received. If there are no corrections, a response is still required.

RETURNING CORRECTIONS:

Corrections must be returned using the ASME Proof Download & Corrections Submission Site (link above). You will be able to upload:

1. Annotated PDF
2. Text entry of corrections, with line numbers, in the text box provided
3. Additional files, if necessary.

SPECIAL NOTES:

Your Login and Password are valid for a limited time. Please reply within 48 hours.

Corrections not returned through the above website will be subject to publication delays.

This e-proof is to be used only for the purpose of returning corrections to the publisher.

If you have any questions, please contact: asme.cenveo@cenveo.com, and include your article no. (GTP-16-1369) in the subject line. This email should not be used to return corrections.

Approval of these proofs re-confirms the copyright agreement provision that all necessary rights from third parties for any copyrighted material (including without limitation any diagrams, photographs, figures or text) contained in the paper has been obtained in writing and that appropriate credit has been included.

Sincerely,

Mary O'Brien, Journal Production Manager

STATEMENT OF EDITORIAL POLICY AND PRACTICE

The Technical Committee on Publications and Communications (TCPC) of ASME aims to maintain a high degree of technical, literary, and typographical excellence in its publications. Primary consideration in conducting the publications is therefore given to the interests of the reader and to safeguarding the prestige of the Society.

To this end the TCPC confidently expects that sponsor groups will subject every paper recommended by them for publication to careful and critical review for the purpose of eliminating and correcting errors and suggesting ways in which the paper may be improved as to clarity and conciseness of expression, accuracy of statement, and omission of unnecessary and irrelevant material. The primary responsibility for the technical quality of the papers rests with the sponsor groups.

In approving a paper for publication, however, the TCPC reserves the right to submit it for further review to competent critics of its own choosing if it feels that this additional precaution is desirable. The TCPC also reserves the right to request revision or condensation of a paper by the author or by the staff for approval by the author. It reserves the right, and charges the editorial staff, to eliminate or modify statements in the paper that appear to be not in good taste and hence likely to offend readers (such as obvious advertising of commercial ventures and products, comments on the intentions, character, or acts of persons and organizations that may be construed as offensive or libelous), and to suggest to authors rephrasing of sentences where this will be in the interest of clarity. Such rephrasing is kept to a minimum.

Inasmuch as specific criteria for the judging of individual cases cannot, in the opinion of the TCPC, be set up in any but the most general rules, the TCPC relies upon the editorial staff to exercise its judgment in making changes in manuscripts, in rearranging and condensing papers, and in making suggestions to authors. The TCPC realizes that the opinions of author and editor may sometimes differ, and hence it is an invariable practice that no paper is published until it has been passed on by the author. For this purpose page proofs of the edited paper are sent to the author prior to publication in a journal. Changes in content and form made in the proofs by authors are followed by the editor except in cases in which the Society's standard spelling and abbreviation forms are affected.

If important differences of opinion arise between author and editor, the points at issue are discussed in correspondence or interview, and if a solution satisfactory to both author and editor is not reached, the matter is laid before the TCPC for adjustment.

Technical Committee on Publications and Communications (TCPC)
Reviewed: 05/2012

AUTHOR QUERY FORM

ASME SETTING THE STANDARD	**Journal: J. Eng. Gas Turbines Power** **Article Number: GTP-16-1369**	**Please provide your responses and any corrections by annotating this PDF and uploading it to ASME's eProof website as detailed in the Welcome email.**

Dear Author,

Below are the queries associated with your article; please answer all of these queries before sending the proof back to Cenveo. Production and publication of your paper will continue after you return corrections or respond that there are no additional corrections.

Location in article	Query / Remark: click on the Q link to navigate to the appropriate spot in the proof. There, insert your comments as a PDF annotation.
AQ1	Reminder – the ASME Copyright Agreement that was signed by all authors includes the following: "You have the right to enter into this Copyright Form and to make the assignment of rights to ASME. If the Paper contains excerpts from other copyrighted material (including without limitation any diagrams, photographs, figures or text), you have acquired in writing all necessary rights from third parties to include those materials in the Paper, and have provided appropriate credit for that third-party material in footnotes or in a bibliography." As required, ASME may contact the authors to obtain a copy of the written permission.
AQ2	Any content obtained from the web and included in the paper may require written permission and appropriate credit if it is copyrighted content. If copyright status cannot be determined, this content should not be included in the paper.
AQ3	Your paper is over 9 typeset pages and is therefore subject to mandatory page charges. An invoice will follow.
AQ4	Please provide either paper number or page number in range for Refs. 26.
AQ5	Please provide DOI or website to access the Ref. 3, 4, 6, 8, 19, 20, 28
AQ6	Please provide Issue or website to access the Ref. 19, 20, 28.

Thank you for your assistance.

J_ID: GTP DOI: 10.1115/1.4034968 Date: 18-October-16 Stage: Page: 1 Total Pages: 14

AQ1
AQ2

AQ3

An Innovative Method for the Evaluation of Particle Deposition Accounting for Rotor/Stator Interaction

Nicola Aldi
Dipartimento di Ingegneria,
Università degli Studi di Ferrara,
Ferrara 44122, Italy

Mirko Morini
Dipartimento di Ingegneria Industriale,
Università degli Studi di Parma,
Parma 43121, Italy

Michele Pinelli
Dipartimento di Ingegneria,
Università degli Studi di Ferrara,
Ferrara 44122, Italy

Pier Ruggero Spina
Dipartimento di Ingegneria,
Università degli Studi di Ferrara,
Ferrara 44122, Italy

Alessio Suman
Dipartimento di Ingegneria,
Università degli Studi di Ferrara,
Ferrara 44122, Italy

Solid particle ingestion is one of the principal degradation mechanisms in the compressor and turbine sections of gas turbines. In particular, in industrial applications, the microparticles not captured by the air filtration system can cause deposits on blading and, consequently, result in a decrease in the compressor performance. This paper presents three-dimensional numerical simulations of the microparticle ingestion (0.15–1.50 μm) in a transonic axial compressor stage, carried out by means of a commercial computational fluid dynamic code. Particles of this size can follow the main air flow with relatively little slip, while being impacted by the flow turbulence. It is of great interest to the industry to determine which zones of the compressor blades are impacted by these small particles. Particle trajectory simulations use a stochastic Lagrangian tracking method that solves the equations of motion separately from the continuous phase. A particular computational strategy is adopted in order to take into account the presence of two subsequent annular cascades (rotor and stator) in the case of particle ingestion. The proposed strategy allows the evaluation of particle deposition in an axial compressor stage, thanks to its capability of accounting for rotor/stator interaction. NASA Stage 37 is used as a case study for the numerical investigation. The compressor stage numerical model and the discrete phase model are set up and validated against the experimental and numerical data available in the literature. The blade zones affected by the particle impact and the kinematic characteristics of the impact of micrometric and submicrometric particles with the blade surface are shown. Both blade zones affected by the particle impact and deposition are analyzed. The particle deposition is established by using the quantity called sticking probability, adopted from the literature. The sticking probability links the kinematic characteristics of particle impact on the blade with fouling phenomenon. The results show that microparticles tend to follow the flow by impacting at full span with a higher impact concentration on the pressure side of rotor blade and stator vane. Both the rotor blade and stator vane suction side are only affected by the impact of smaller particles (up to 1 μm). Particular fluid dynamic phenomena, such as separation, shock waves, and tip leakage vortex, strongly influence the impact location of the particles. The kinematic analysis shows a high tendency of particle adhesion on the suction side of the rotor blade, especially for particles with a diameter equal to 0.15 μm. [DOI: 10.1115/1.4034968]

Introduction

Each manufacturer's gas turbine has its own tolerances and design constraints, each use its own operational requirements and each installation site its own particular climatic conditions. In any case, in each location gas turbines are involved in performance degradation.

Fouling represents a degradation which is generally recoverable with cleaning/washing operations. Therefore, axial compressor fouling is a serious operating problem, and its control is of critical importance for operators of gas turbine-driven power plants, compressor stations, and pump stations.

The fouling mechanism involves three specific aspects: (i) the environmental conditions (airborne contaminant, salt, etc.) in which the gas turbine operates, (ii) the power plant design and management (filtration system, washing operations, etc.), and (iii) compressor characteristics (pressure ratio, number of stages, etc.). These aspects work together determining the fouling mechanism. For industrial gas turbines, highly effective filtration systems exist [1]. Depending on the type of filtration system used, smaller particles (<2 μm) can enter the engine. These smaller particles are too small to cause erosion, but they do cause compressor fouling. Evaluations of fouled compressors have revealed contamination both on the pressure side and the suction side of the compressor blades [2].

In order to carry out a comprehensive analysis of the fouling issue, both numerical studies and experimental approaches should consider the sticking capability of particles. Theoretically, zones with a high number of impacts will be more affected by the fouling phenomenon but, in practice, fouling depends only on the sticking characteristic of particles. The particle sticking on the blade surface results in an increase of the thickness of the airfoil and of the surface roughness. Both these events change the flowpath inside the blade passages, causing (i) an increment of the boundary layer thickness, (ii) a decrement of the flow passage area, and (iii) modifications of the 3D fluid dynamic phenomena.

Particle adhesion on the blade surface is a complex phenomenon that includes many aspects: (i) the material of the body in contact, (ii) the surface conditions, (iii) the particle size, (iv) the impact velocity, and (v) the impact angle. In this paper, the authors present a numerical study for the ultra-fine powder ingestion by a transonic axial compressor stage. This work is the development of the analyses reported in Refs. [3] and [4], in which the CFD simulation is applied to a rotor cascade only for defining

Contributed by the Oil and Gas Applications Committee of ASME for publication in the Journal of Engineering for Gas Turbines and Power. Manuscript received July 28, 2016; final manuscript received August 26, 2016; published online xx xx, xxxx. Editor: David Wisler.

which blade areas are more affected by the particle impact and adhesion. In this paper, the particle ingestion and the subsequent particle deposition on the entire stage are studied by using CFD simulations and a postprocess computational strategy, which allows the rotor/stator interaction to be considered. The main phases of this work are summarized below:

- validation of the numerical model of the compressor stage by means of performance curves available in the literature;
- simulation of the ingestion of a fine powder characterized by three different particle diameters (0.15 μm, 0.50 μm, and 1.50 μm). The simulation of particle ingestion is performed separately for the rotor and the stator cascades;
- determination of the kinematic characteristics (velocity and angle) of particles that impact on the rotor blade and stator vane according to pressure side and suction side subdivision;
- estimation of the sticking probability for each particle that impacts the rotor blade and stator vane in order to define the preferable deposition zones as a function of the particle diameter;
- application of a postprocess strategy for considering the effect exerted by the rotor blade on the deposition zone location of the stator vane surface.

Literature Review

The results of fouling detection in single or multistage compressors have been featured in the literature since 1950s [5]. A thorough literature review of experimental studies with regard to the deposition on axial compressor blade surfaces is reported in Refs. [3], [4], and [6]. Tarabrin et al. [7] highlight that the deposit amount is greater on the stator vanes than on the rotor blades due to the cleaning effects provided by the centrifugal forces on dirt particles. Centrifugal force effects also characterize the results obtained by Syverud et al. [8]. The tests show that the salt deposits are mainly found along the leading edge of the first four stages and on the pressure side of the stator vanes along the hub. The salt deposits are generated by salt particles (<2 μm) carried by water droplets and, for this reason, significantly less deposit is observed on the rotor blades compared to the stator vanes.

The question that still requires research is the mechanism through which particles reach the suction surface. Particles that deviate from the streamlines will readily impact on the pressure side of the blades, but the mechanism that can deposit particles on the suction side of the blade is not fully understood. Starting from these considerations, the possibilities for investigating particle kinematics are linked to: (i) the abilities to use numerical simulations and/or experimental tests for studying the fouling phenomenon and (ii) the knowledge of how particles are able to stick to blade surface.

Numerical simulations of particle behavior in axial compressor cascades can be found in Refs. [3], [4], and [6]. The authors analyze the microparticle trajectories in a transonic [3,4] and in a subsonic [6] rotor, in order to discover which blade zones are affected by particle impact and adhesion. In order to numerically investigate particle ingestion in an axial compressor stage, particles must be tracked in both the rotating frame of the rotor domain and the stationary frame of the stator domain, passing through an interface which couples the rotor and the stator cascades. In a recent work, Zagnoli et al. [9] report a review of the computational studies performed in past years tracking different types of particles through compressor and turbine stages. In these works, most of which deal with erosion in compressors [10,11] and turbines [12–14], and steady (mixing plane and frozen rotor) and unsteady models are employed at the interface between rotating and stationary domains for the rotor/stator coupling. The authors in Ref. [9] study deposition in the first stage of a high-pressure turbine using both steady mixing plane and unsteady sliding mesh calculations, in order to observe differences due to particle size (3–15 μm) and computational methods. Steady methods are found to over-predict impacts and deposits relative to unsteady methods by averaging out discrete unsteady vane wake motion, which causes particle motion toward blade surfaces.

Methodology

The methodology adopted here for analyzing particle ingestion in an axial compressor stage is different from that reported in the literature [9–14]. In this case, in fact, particles are not tracked through the interface between rotating and stationary domains, but the analysis is carried out by means of separate particle injections for the isolated rotor and stator cascades.

The flow field within the entire compressor stage is initially simulated, with the stage operating at the best efficiency point at the rotor design rotational speed. The coupling between the rotor and the stator is obtained through a mixing plane interface, modeling a single passage per cascade.

After this preliminary calculation, the flow field is solved for the isolated rotor and stator. The flow simulation setup for the rotor and the stator is performed by using the same boundary condition types considered for the stage simulation. Radial profiles of flow variables calculated in the stage simulation are exported at the level of the mixing plane interfaces and imposed at the inflow and outflow boundaries of the isolated rotor and the stator, respectively. Then, the CFD solver is run for the two cascades separately. In this way, the flow conditions within the individually simulated rotor and stator match those resulting from the entire stage simulation.

Particle injections for the isolated rotor and stator take place on the previously solved flow field. Particles are released at the same local velocities as the air flow from an inlet radial plane with equally spaced injection points for both the rotor and the stator. The uniform distribution of injection points allows the realization of a uniform particle injection from the inlet section of each cascade. Moreover, since the number of rotor blades is different from that of stator vanes and only a single passage per cascade is modeled, rotor and stator domains are characterized by different pitch angles. For these reasons, the total number of injected particles is different for the two cascades.

The study of particle impact and adhesion on the rotor blade and stator vane is carried out by subdividing the flow channel of the individual cascades into 11 annular stream tubes of the same radial extent. In this way, 11 radial bands of equal width are identified at the inlet and outlet sections of each cascade, and the rotor blade and stator vane are divided along the spanwise direction into 11 strips. In accordance with a uniform particle injection, the number of particles injected from each inlet radial band depends on the band area only and increases from the inner to the outer band, since the band area increases.

For the isolated rotor and stator, the location and the kinematic characteristics of particle impact on the blade surface are determined. These data are then used to estimate the sticking probability of particles that impact on the rotor blade and stator vane, allowing for the definition of the preferable deposition zones.

Finally, the results of the isolated rotor and stator characterizations are postprocessed in order to take into consideration the effect of the interaction between the rotor blade and the particles while analyzing deposition on the stator vane. The adopted postprocess computational strategy is based on the following assumptions:

- the number of particles that stick to the rotor blade (i.e., particles characterized by a sticking probability greater than 0.5) is negligible with respect to the total number of injected particles. This approximation is justified by the data reported in Table 1. The particles uniformly injected from the rotor inlet section are thus simply redistributed by the cascade internal flow;
- the particles released from each radial band of the stator inlet section can deposit exclusively on the corresponding strip of

Table 1 Injected and stuck particles for the isolated rotor

d_p (μm)	0.15	0.50	1.50
Injected particles	3,031,305	2,963,849	3,029,539
Stuck particles	45,710	52,402	97,634

the stator vane. This implies that the entity of particle radial motions within the individual annular stream tube is such that particles cannot pass to an adjacent stream tube. This hypothesis is considered acceptable, since the analysis is performed at the stage best efficiency point, where no significant radial flows occur, as shown in Fig. 1.

On the basis of the previous assumptions, a linear relationship between the number of particles injected from each band of the stator inlet section and the number of particles adhering to the stator vane corresponding strip is assumed. Therefore, the effect of the rotor presence is considered as a magnification/reduction of the adhesions of particles leaving the stator inlet section from each band, according to the particle radial distribution obtained at the rotor outlet section. This strategy is schematically illustrated in Fig. 2.

Stage Numerical Model and Validation

In order to investigate the microparticle ingestion and adhesion in an axial compressor stage, the NASA Stage 37 is used as the case study geometry. The stage geometry and performance data are gathered from Ref. [15].

Reference Numerical Compressor Stage. The NASA Stage 37 consists of a rotor and a stator. The rotor is composed of 36 blades, and the tip clearance at design speed is 0.356 mm (0.45% of the blade span). The stator is composed of 46 vanes, and the hub clearance is not present. To reduce the computational effort, only a single passage per cascade is modeled, as can been seen in Fig. 3.

Numerical Grid. The grid used in the calculations is a hexahedral grid with a total number of 2,201,776 elements. The grid is realized by employing an O-grid around both rotor blade and stator vane surfaces, with local refinements near the hub and shroud regions. The meshes on the rotor blade and stator vane surfaces are shown in Figs. 3(*b*) and 3(*c*), respectively. The first grid points on the rotor blade and stator vane surfaces and end walls are positioned in such a way that the y^+ values range from 5 to 100.

In the tip region, the grid is split along the center of the rotor blade thickness, and the nodes do not match across the two halves. Here, the mesh is connected using a nonconformal interface. The rotor tip clearance is resolved with four nodes across the gap span.

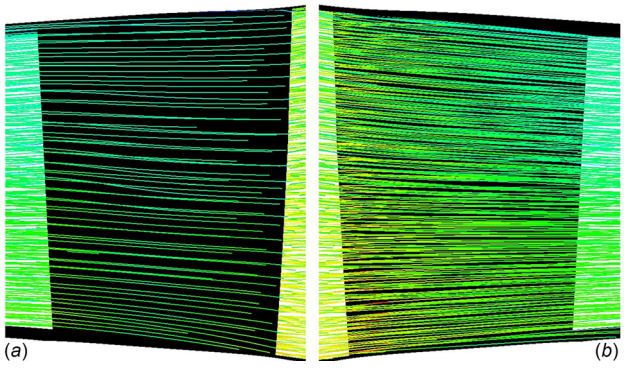

Fig. 1 Streamline pattern within the isolated stator: (*a*) pressure side and (*b*) suction side

Numerical Code. The numerical simulations are carried out by means of the commercial CFD code ANSYS Fluent 15.0 [16]. The code solves the 3D Reynolds-averaged form of the Navier–Stokes equations by using a finite-volume method. The density-based solver with the implicit solution formulation and Roe-FDS convective flux type is used. For gradient discretization, the Green-Gauss node-based method is selected. A second-order upwind discretization scheme is adopted for flow equations.

Turbulence Model. The turbulence model used in the calculations is the standard k–ε model, and near-wall effects are modeled by means of standard wall functions. A first-order upwind discretization scheme is selected for both turbulent kinetic energy and turbulent dissipation rate equations.

Rotor/Stator Interaction Model. All the compressor stage simulations are performed in a steady multiple reference frame in order to take into account the contemporary presence of moving and stationary domains. A mixing plane model is imposed at the interface between rotating and stationary domains, each of which is solved as a steady-state problem with its own inlet and outlet boundary conditions. The mixing plane interface, whose geometry is radial, is composed by the coupling of an upstream rotor outlet boundary with a downstream stator inlet boundary. The flow-field data at the mixing plane interface are averaged in the circumferential direction on both rotor outlet and stator inlet boundaries. In particular, the mixed-out averaging method provided by the ANSYS Fluent is chosen. The mixed-out average is based on the conservation of mass, momentum and energy, and it is therefore considered a better representation of the flow since it reflects losses associated with nonuniformities in the flow profiles. By performing circumferential averages of flow properties at rotor outlet and stator inlet boundaries, profiles of flow variables are defined as a function of the radial coordinate. Radial profiles computed at the rotor outlet are used to update boundary conditions at the stator inlet and vice versa during the calculation process.

The computational domain consists of four fluid domains: three stationary domains (inlet duct, stator and outlet duct) and one rotating domain (rotor). Each domain is coupled with the adjacent one through a mixing plane interface. Passing radial profiles of flow variables from adjacent domains in the manner described above requires specific boundary condition types to be defined at the mixing plane interface. All the stage simulations are carried out by assigning pressure outlet and pressure inlet boundary condition types to the upstream and downstream sides of each mixing plane interface, respectively. Swirl and total enthalpy conservation is also enforced across the mixing plane interfaces.

Properties and Boundary Conditions. An ideal gas approximation is used for air. It is also assumed that the fluid has a constant specific heat, thermal conductivity and viscosity.

The total pressure, total temperature, and flow direction are assigned to the inflow boundary of the inlet duct. The inlet total pressure $p_{0,1}$ and total temperature $T_{0,1}$ are set equal to 101,325 Pa and 288.15 K, respectively. The flow is defined to be normal at the inflow boundary. Turbulence parameters are specified at the inlet section in terms of turbulence intensity and turbulent viscosity ratio, which are set equal to 5% and 10, respectively.

An average relative static pressure $p_{g,3}$ is imposed at the outflow boundary of the outlet duct, both in the near-choked flow region and in the near-stall region, with radial equilibrium pressure distribution. The outflow pressure is progressively increased in order to reproduce the entire performance trend.

Rotor blade and stator vane surfaces and end walls are modeled as no-slip, smooth, and adiabatic walls. All the simulations refer to the rotor design rotational speed, equal to 17,188 rpm. Furthermore, since only a section of the full geometry is modeled, rotational conformal periodic boundary conditions are applied to the lateral surfaces of the flow domain.

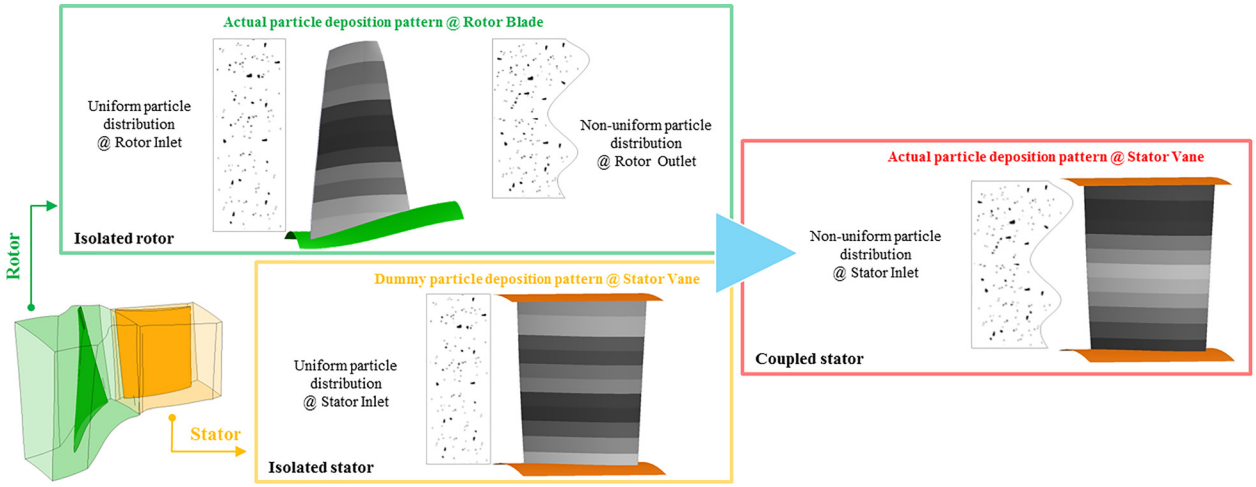

Fig. 2 Schematic illustration of the adopted postprocess computational strategy

The results presented in this paper are obtained from convergent simulations, with a variation of the residues of the motion and turbulent equations close to zero and all lower than 10^{-4}.

Validation. The validation of the numerical model of the compressor stage is performed by means of comparison with experimental measurements gathered from Ref. [15]. This comparison is carried out taking into consideration the total pressure ratio β and the adiabatic efficiency η as a function of the mass flow rate m. The numerical and experimental performance curves are reported in Fig. 4. It can be noticed that the shape of both the experimental performance curves is correctly reproduced by the numerical model. Since the aim of the validation is to obtain a reliable compressor stage model, the validation of the numerical model can be considered acceptable. The numerical results are in fairly good agreement with the experimental data. The deviation in terms of mass flow rate at the choked-flow condition is about 3.34%.

Particle Model

The solution approach is based on a mathematical model with Eulerian conservation equations for the continuous phase and a Lagrangian frame to simulate a discrete second phase. In this approach, the airflow field is first simulated, and then, the trajectories of individual particles are tracked by integrating a force balance equation on the particle.

Balance of Forces. The force balance is comprehensive of inertia, drag, and buoyancy terms. In the force balance, there are two contributes due to the shear stress and diffusion called Saffman's lift force and Brownian force, but these two contributes become important in very few cases. In this analysis, only the Brownian term is neglected. An extensive description of the force balance is reported in Ref. [3].

Near-Wall Particle Behavior. For the particle–wall interaction boundary conditions, a nonadherence condition (named *reflect*) is imposed on the rotor blade and stator vane surfaces and end walls. Specific functions and restitution coefficients for the near-wall particle behavior are implemented by the authors. The model functions are defined in agreement with Ahlert's model [17] and Forder's coefficients [18]. In a general application, restitution coefficients could depend on (i) impact velocity, (ii) pressure, and (iii) temperature [19]. In this case, only the velocity could represent an obstacle through the correct representation of the particle bounce. The restitution coefficients used in this study are obtained from Forder's work [18], in which an oilfield control valve is studied with a flow velocity almost equal to 80 m/s. This velocity value determines the validity of assuming the restitution coefficients independent from the velocity.

Particle Injection. The particle density ρ_p is set equal to 2560 kg/m^3, and the variation of the particle diameter d_p is in the range of 0.15–1.50 μm, while the Stokes number (Eq. (1)), calculated at the rotor and stator inlet sections, is in the range of 0.0002–0.04

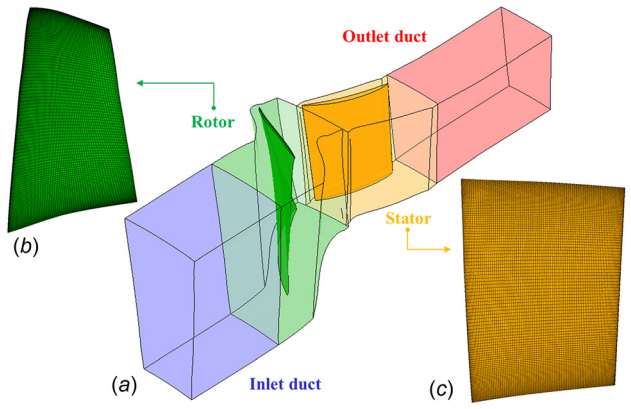

Fig. 3 NASA Stage 37 computational domain: (*a*) single passage model, (*b*) mesh on rotor blade surface, and (*c*) mesh on stator vane surface

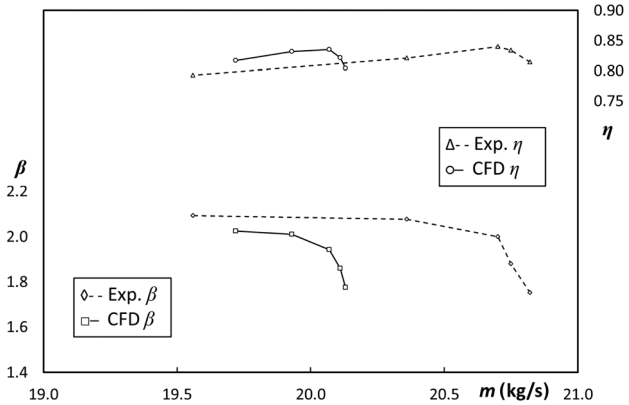

Fig. 4 Comparison between the experimental results (Exp.) [15] and CFD results (CFD)

$$\mathrm{St} = \frac{\rho_p d_p^2}{18\mu}\frac{U_1}{d_h} \quad (1)$$

Particles are spherical and nondeformable. All the analyses refer to injections having particles with the same diameter, the same material, and thus, characterized by the same Stokes number. On the other hand, the total mass flow rate of the discrete phase, m_p, is linked to the air flow rate and the contaminant concentration. The latter is related to the work environment of the compressor and the efficiency of the filtration system η_f. Since rotor and stator domains are characterized by different pitch angles (and, therefore, elaborate different air flow rates), a different value of total mass flow rate of contaminants is imposed at the inlet sections of the rotor and the stator. Moreover, it is assumed that particles do not affect the fluid flow (one-way coupling) as the particle's volume fraction is very low ($\ll$10%). The injection data for the isolated rotor and stator cascades are summarized in Table 1.

Particle Turbulent Dispersion. The turbulent dispersion of particles in the fluid phase can be predicted by using a stochastic tracking model. The time-averaged flow field determines the mean path of particles, while the instantaneous flow field governs each particle's turbulent dispersion from the mean trajectory. By computing the trajectory in this manner for a sufficient number of particles, the random effects of turbulence on particle dispersion can be included.

This investigation uses the discrete random walk (DRW) model to simulate the stochastic velocity fluctuations in the airflow. The DRW model assumes that the fluctuating velocities follow a Gaussian probability distribution. This model may give nonphysical results in strongly nonhomogeneous diffusion-dominated flows, where small particles should become uniformly distributed. Instead, the DRW model will show a tendency for such particles to concentrate in low-turbulence regions of the flow. In this case, a specific analysis conducted by the authors shows that the interaction between the wall, with its boundary layer, and the discrete phase is characterized by the inertial law, as explained in more detail in subsequent paragraphs. For this reason, the diffusion phenomena can be neglected and the DRW model can be considered reliable. The number of tracked particles is selected in order to satisfy the statistical independence, since turbulent dispersion is modeled based on a stochastic process.

The turbulence model plays a key role in the resolution of particle trajectories near the wall. Through the use of the k–ε turbulence model with standard wall functions there is an isotropic treatment of the turbulence near the wall, and this implies, in the case where the values of y^+ are less than 5, that both the streamwise mean velocity and the turbulent kinetic energy will be overestimated [20]. In this study, as mentioned above, the values of y^+ do not drop below 5.

In Ref. [20], the authors report an extensive sensitivity analysis of the relationship between turbulence models, mesh refinement close to the wall, and particle dimensions expressed by the nondimensional particle relaxation time τ^+, defined as

$$\tau^+ = \frac{(\rho_p/\rho)d_p^2 u_t^2}{18\nu^2} \quad (2)$$

where u_t is the shear velocity

$$u_t = \sqrt{\frac{\tau_w}{\rho}} \quad (3)$$

and τ_w is the wall shear stress. Tian and Hamadi [20] highlight the effect of a different turbulence model on the velocity deposition for particles in a horizontal and vertical tube. Their study shows that the k–ε turbulence model with standard wall functions overpredicts the deposition velocity for particles in a *Brownian* ($\tau^+ < 10^{-2}$) and *transition* ($10^{-2} < \tau^+ < 10$) region, and it does not allow the estimation of the real trend of the particle velocity deposition. For the *inertial* ($\tau^+ > 10$) region, the k–ε turbulence model with standard wall functions over-predicts the deposition velocity, but in a minor way compared to the other regions, and the trend of the deposition velocity curve is in agreement with the other results.

As can be seen in Table 2, the nondimensional particle relaxation time τ^+ for the simulations presented in this paper is in the range 2–252, which corresponds to the *transition* and *inertial* region in accordance with Ref. [20]. For this reason, the k–ε turbulence model with standard wall functions used for all the analyses is considered suitable for studying the real deposition phenomenon that occurs in the axial compressor stage under investigation.

Isolated Rotor/Stator Characterization

In this paragraph, the results of the characterizations of the isolated rotor and stator cascades are reported. Starting from the analysis of the kinematic characteristics of particle impact on the blade surface, the zones characterized by a high probability of particle deposition are identified by means of the sticking probability calculation.

Impact Analysis. Only a portion of particles injected from the inlet section of each cascade impacts on the rotor blade and stator vane. For comparison among the studied cases, the ratio η_{hit} can be used. η_{hit} is defined as the ratio between the number of particles that hit the blade and the total number of injected particles. The trend of η_{hit} as a function of the particle diameter d_p is shown in Fig. 5. It is possible to observe that the percentage of particles that hit the blade surface increases with the particle diameter for both the rotor and the stator. The number of particles that impact the rotor blade is very similar to the number of particles that impact the stator vane, and the two trends are very close to each other. In Fig. 5, the total number of injected particles and the absolute number of impacting particles on the blade surface are also reported for all the studied cases. The results related to the rotor blade impacts are in line with those presented in the previous work [3].

Regarding the particle impact location on the blade surface, Fig. 6 shows the trends of the impacting particles on the rotor blade and the stator vane for all the considered particle diameters: (i) the η_{hit} values for the pressure side, $\eta_{hit,PS}$, and suction side, $\eta_{hit,SS}$, refer to the percentage of particles that hit the pressure side or suction side compared to the total number of injected particles, while (ii) the η_{side} values, reported in pie charts, represent the percentage of particles that hit the blade on the pressure side or suction side compared to the total number of particles that hit the blade.

From the analysis in Fig. 6, it can be seen that by increasing the particle diameter the number of particles that hit the pressure side increases in the same manner for the rotor blade and stator vane. For the suction side, the rotor blade trend decreases as the particle diameter increases. In the case of the stator vane, the number of particles that hit the vane with a diameter equal to 1.50 μm is higher than that of particles with a diameter equal to 0.50 μm. The differences in the impact trends highlighted for the rotor and stator are due to the different shape of their airfoils. The stator airfoils have a thicker leading edge, resulting in a higher capability of collecting particles. These results agree with those presented in Ref. [6], where a subsonic rotor blade is analyzed. Considering the pie charts, the results are in line with those reported in the literature in the case of (i) fouling due to particles with dimensions close to the unit of micron [2] and (ii) erosion of rotor blades (which involves larger particles) [11]. In fact, the fouling phenomenon is characterized by a wider distribution of the particles on the blade surface with respect to erosion, which shows a higher percentage of impacts on the pressure side than on the suction side. In Appendix A, an overall representation of the impact zones is

Table 2 Injection data for the isolated rotor and stator

	Rotor			Stator		
d_p (μm)	0.15	0.50	1.50	0.15	0.50	1.50
Stokes number, St	2×10^{-4}	2×10^{-3}	3×10^{-2}	4×10^{-4}	5×10^{-3}	4×10^{-2}
Nondimensional relax. time, τ^+	3	28	252	2	19	167
Filtration eff., η_f (%)	61	65	96	61	65	96
Mass flow rate, m_p (kg/s)	7.3×10^{-7}	2.4×10^{-5}	7.5×10^{-5}	4.3×10^{-7}	1.4×10^{-5}	4.3×10^{-5}

illustrated for some representative airfoils for both the rotor blade and the stator vane.

The modules of the particle impact velocity v_i are reported in Fig. 7 for the rotor blade and the stator vane. The velocity values refer to the vector sum of the three velocity components along the coordinate axes at the impact point on the blade surface. Each dot is colored by the impact velocity and it is superimposed with respect to the mesh node that provides the blade shape.

For the rotor blade, the effect of the separation that occurs on the suction side and the impact velocity peaks that take place at the blade tip area are clearly visible. The shock wave causes the drop in the particle impact velocity, and at about 50% of the chord it is possible to find the lowest impact velocity. The stator vane shows different impact velocity patterns. The impact velocity peak is located close to the hub in the first part of the airfoil chord for both the pressure and suction side, while the impact velocity assumes the lowest values in the vane region close to the shroud, where a flow separation takes place. The flow separation influences the particle impact velocity on the suction side near the end walls. In particular, local three-dimensional phenomena affect the particle trajectories. Flow separation in the corner region of the vane passage is common in axial compressors, as reported by Gbadebo et al. [21]. Moreover, Fig. 7 shows that particle impact velocities are very different on the same side of the blade. These differences are due to the shape of the blade (e.g., blade height) and the fluid dynamic phenomena (e.g., flow separation).

The impact velocity is not the only parameter needed to determine particle adhesion on the blade surface. As mentioned above, particle adhesion is due to a combination of different effects, but the most important parameters are the normal v_n and tangential v_t impact velocity components. Therefore, the particle impact angle α, which is the angle between the surface normal vector and the impact velocity vector, is analyzed in order to better understand the kinematic characteristics of particle impact.

In Fig. 8, the particle impact angle is reported by means of a colored particle plot. In some instances the impact angle is greater than 90 deg. This is due to (i) the surface local curvature (e.g., at the leading and trailing edges) and (ii) surface reconstruction approximation during the particle impact postprocess [4,6]. A deviation can arise from the fact that the surface is reconstructed by interpolating points on the mesh elements in the vicinity of the point of impact. The approximation introduced by this procedure is considered acceptable by the authors, allowing for a confidence band of ± 5 deg for all the results presented in this paper. Figure 8 illustrates that the impact angle assumes the widest variation at the leading and trailing edges, due to the surface curvature of the rotor blade and stator vane. For the pressure side, the rotor blade shows impact angle values close to 90 deg (i.e., particles are tangential to the blade surface) and, by contrast, the stator vane shows impact angle values close to 0 deg (i.e., particles are perpendicular to the blade surface). The suction side presents almost the same impact angle values for both the rotor blade and stator vane, even if, for the rotor blade, the effects of flow separation are still visible.

Adhesion Analysis. A quantitative analysis of particle adhesion on the isolated rotor, and stator is provided by using the experimental results found in Ref. [22], in which particle velocity and materials are among the most similar to the particles causing the fouling phenomenon. As the authors in Refs. [4], and [6] previously showed, starting from the experimental sticking probability trends reported in Ref. [22], it is possible to define representative trends for the correlation between the normal

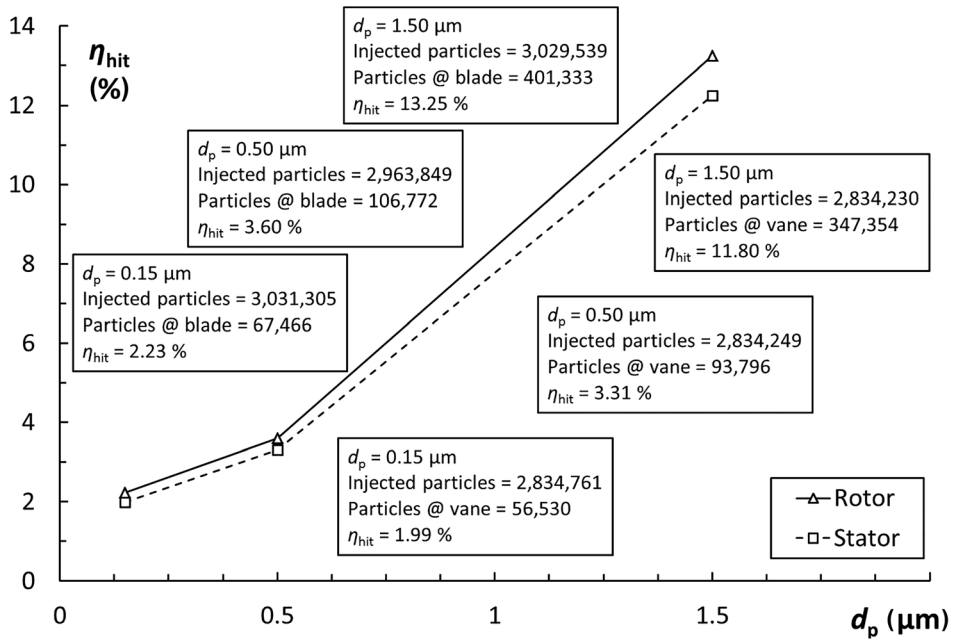

Fig. 5 Capture efficiency versus particle diameter for the isolated rotor and stator

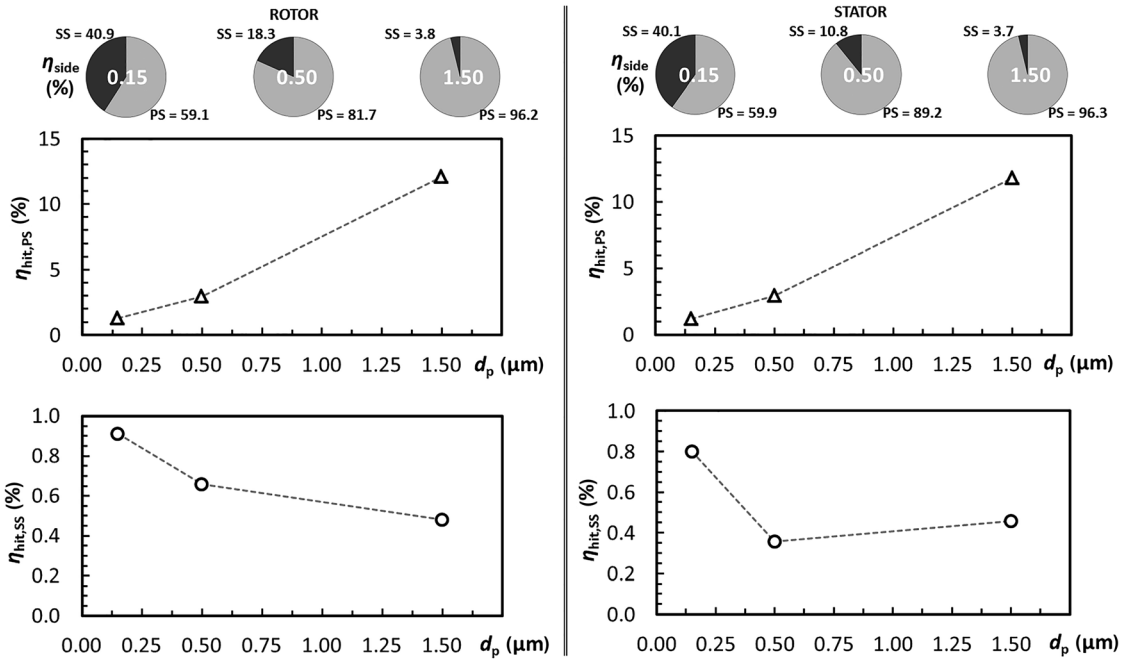

Fig. 6 Particle impact distributions for the isolated rotor and stator

impact velocity v_n and the sticking probability SP. The modules of v_n are shown in Appendix B for the rotor blade and the stator vane. For particle diameters lower than 0.50 μm, the equation that links v_n with SP for lower normal impact velocities (<4 m/s) is

$$S_p = -0.09v_n + 0.99 \quad (4)$$

while for higher impact velocities (4–90 m/s), it is

$$S_p = 2 \times 10^{-6}v_n^3 - 0.000378v_n^2 + 0.011800v_n + 0.587100 \quad (5)$$

In the case of particle diameter higher than 0.50 μm, the equation for lower normal impact velocities (<4 m/s) is

$$S_p = -0.112v_n + 0.990 \quad (6)$$

while for higher impact velocities (4–90 m/s) it is

$$S_p = -6 \times 10^{-5}v_n^2 - 6e - 4v_n + 0.545 \quad (7)$$

On the basis of the previous relations, for smaller particles the sticking probability is equal to 0.5 at a normal impact velocity of 48.35 m/s. Instead, for bigger particles the sticking probability is equal to 0.5 for a normal impact velocity of 22.85 m/s. Therefore, the smaller particles have a wider range of normal impact velocity for which particle impact with the blade surface becomes (with a high probability) a permanent adhesion. Equations (4)–(7) are used to calculate the sticking probability for each particle that impacts on the surface by using the normal impact velocity.

Because of the particle-wall interaction settings, particles do not stick to the surfaces. Particles bounce on the rotor blade, stator vane, and end walls following the rules imposed by the restitution coefficients. In the literature, some studies can be found on the effects of the particle bounce especially related to erosion phenomena [10]. Bouncing particles possess high kinetic energy, that

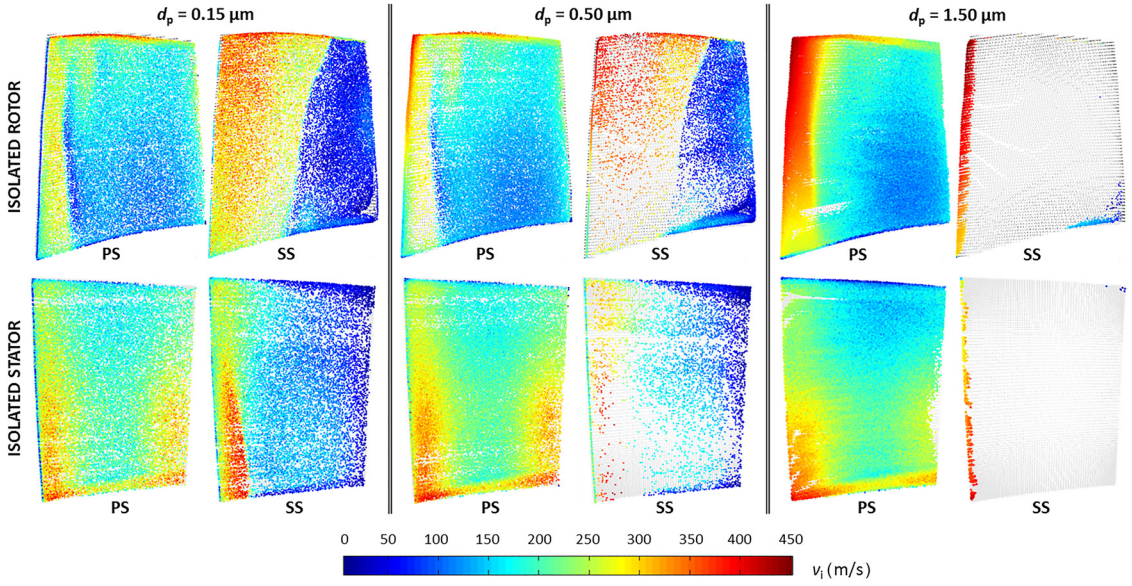

Fig. 7 Particle impact velocity for the isolated rotor and stator

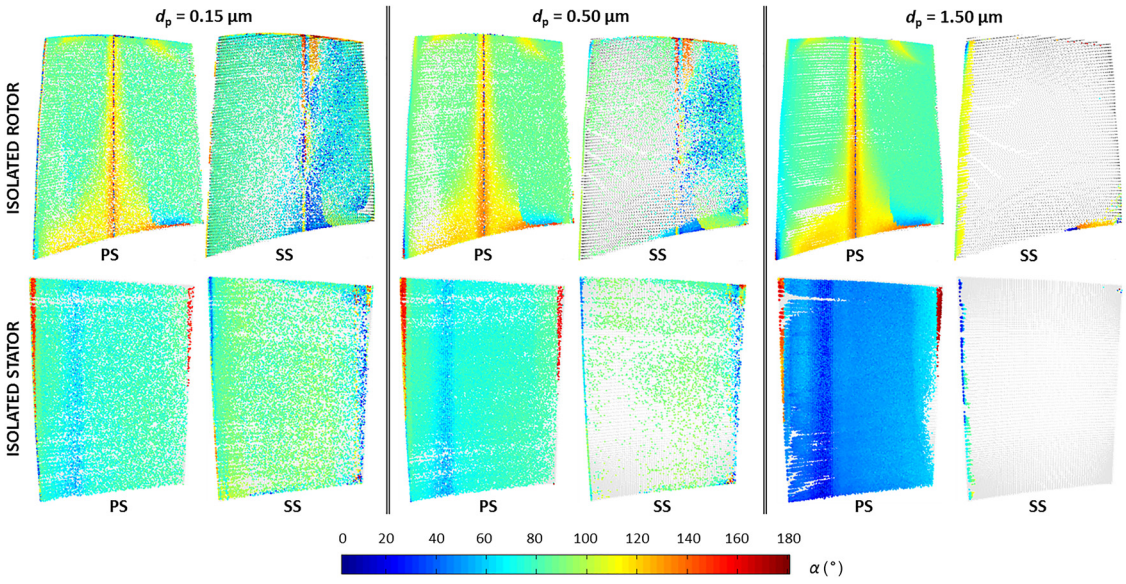

Fig. 8 Particle impact angle for the isolated rotor and stator

decreases by an order of magnitude during the first impact [22]. Such a phenomenon implies that these particles will not be able to stick during the first contact, but, instead, it will most likely be during the second one. In fact, the decrease in kinetic energy is related to the decrease in velocity and, consequently, to an increase in sticking probability. For this reason, the particle adhesion values take into account the particle bounces. More specifically, the bounces of each particle are analyzed in terms of normal impact velocity and only when the normal impact velocity value allows particle sticking (i.e., the sticking probability is greater than 0.5) the particle is considered stuck to the surface, and the subsequent bounces, if present, are erased.

In Fig. 9, the trend of the ratio $\eta_{\text{hit,SP>0.5}}$ (black continuous line) for particles characterized by a sticking probability greater than 0.5, superimposed with the trend of the ratio η_{hit} (gray dotted line), is reported. The two trends refer to both sides (pressure and suction side) of the rotor blade and stator vane. As can be seen, the trend of $\eta_{\text{hit,PS,SP>0.5}}$ for the pressure side of both the rotor blade and stator vane does not follow the trend of $\eta_{\text{hit,PS}}$, unlike the trends of $\eta_{\text{hit,SS,SP>0.5}}$ for the suction side. For the pressure side, the number of stuck particles is quite independent from the total number of particles that hit the blade and $\eta_{\text{hit,PS,SP>0.5}}$ remains almost the same for the three considered particle diameters. In this case, the larger particles produce more fouling effects due to their greater diameter and thus their greater mass. The two percentages are very close to each other only for the smallest particles, showing the high capability of smaller particles to stick to the blade surface. For the suction side, the trend of the ratio $\eta_{\text{hit,SS,SP>0.5}}$ highlights a very high percentage of particles able to stick for the smallest diameters compared to the total number of particles that hit the suction side. For higher particles, the percentage is very low due to the very low number of particles that reach the suction side.

The particles that stick to the rotor blade and stator vane are shown in Fig. 10 by using black dots. Each dot represents a stuck particle (i.e., a particle for which the sticking probability is greater than 0.5). Smaller particles are able to cover the entire blade surface (pressure and suction side), even though a small portion of the blade close to the leading edge appears free from deposits. Moving to bigger particles, the suction side and certain zones of the pressure side are less affected by particle deposition.

Fluid dynamic phenomena influence the particle deposition patterns as illustrated in Ref. [23], where field data regarding the deposition of foulants on a transonic compressor blade are reported. The authors show the blade surface condition after 25,000 h of operation and highlight that three-dimensional flow features cause small particles to be deposited in zones where secondary flows and vortices are dominant. Figure 11 shows a qualitative comparison between the actual deposits on a rotor blade taken from Ref. [23] and the numerical results of the present analysis (0.50 μm particles). Depending on the blade side, it is possible to observe similar deposition patterns. The effect of the shock wave is clearly visible on the suction side of the blade, where a narrow region which is free from deposit can be detected. For the pressure side, a greater amount of deposits is present in the second part of the blade chord, especially close to the hub and at blade midspan. At the leading edge of the blade, a particular deposition pattern can be seen. The effect of the stagnation determines the high presence of impacting particles on the leading edge and, by contrast, there are no particles in the area immediately downstream. This phenomenon is more evident in the case of smaller particles that impact the rotor blade, where the velocity field could be characterized by normal shock waves due to the local curvature of the airfoil [24]. Regarding the stator vane, the latter phenomenon is still observable and, in this case, the thicker nose of the airfoil determines the blade capability of collecting particles. Similar results can be found in Ref. [8]. The deposition on the leading edge represents a key aspect, because the changes in the leading edge area (shape, size, and surface roughness) are one of the most important causes of performance degradation due to fouling [25] and erosion [26]. Deposit distributions, different from the pressure side and suction side moving to higher particle diameters, agree with those reported in the literature in the case of (i) fouling due to particles with dimensions close to the unit of micron [2] and (ii) erosion of rotor blades (which involves larger particles) [11].

In general, the rotor blade and stator vane show almost the same behavior related to particle sticking, even though the effects on the stage performance are different. As reported by Morini et al. [27], the effects of rotor deposits (e.g., surface roughness and airfoil thickness) on stage performance are greater with respect to those generated by the same amount of deposits on the stator vane.

As described above, the sticking probability defined in Ref. [22] only considers the normal impact velocity. However, in this application particular attention must be paid to the tangential impact velocity v_t. In fact, as can be seen in Appendix B, the magnitude of v_t is not negligible. The tangential impact velocity can reach 250 m/s or 400 m/s on the pressure side and suction side, respectively. These very high velocity values could diminish the sticking probability and transform an adhesion-impact into a

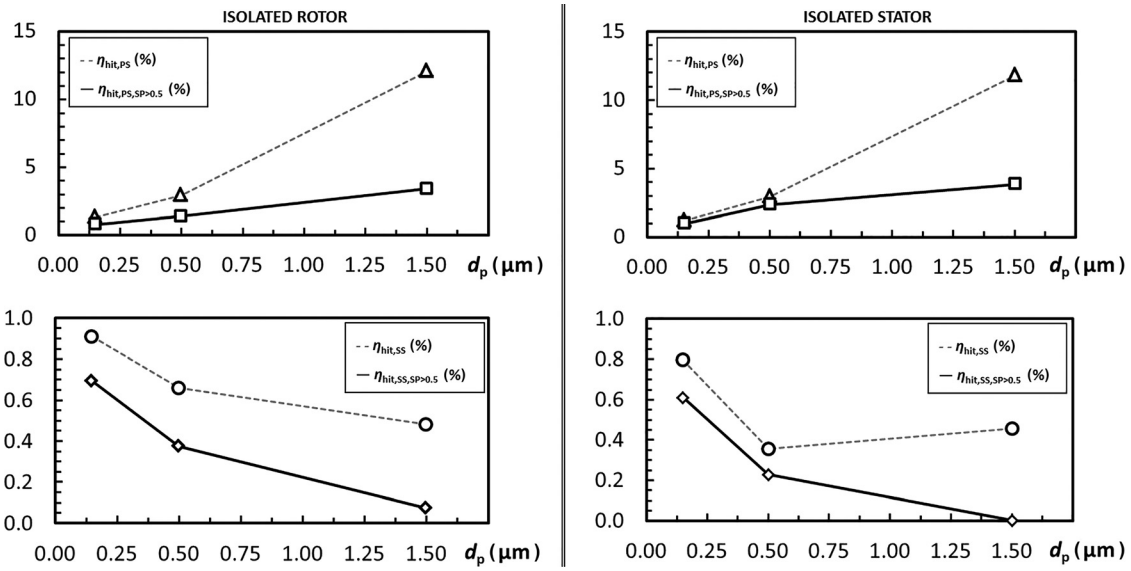

Fig. 9 Trends of the ratio $\eta_{hit,SP>0.5}$ and η_{hit} superimposed for the isolated rotor and stator

slip-impact (specific studies on the interaction between normal and tangential impact velocities are not available in the literature). Conversely, it can be noted that in the suction side separation zone of the rotor blade, the tangential impact velocity is much smaller, thus, limiting the possibility of slip between the particles and blade surface.

Coupled Stator Analysis

The particle deposition patterns for the stator vane shown in Fig. 10, which result from the characterization of the isolated stator cascade, are not representative of the actual deposits, since they are determined starting from a uniform particle injection. Actually, the deposits on the stator vane surface are the consequence of the action exerted by the rotor blade on the particle trajectories. In order to consider the effect of the interaction between the rotor blade and the particles while analyzing deposition on the stator vane, the postprocess computational strategy previously described is applied.

Figure 12 reports the trends of the ratio $\eta_{hit,SP>0.5}$ for both sides of the stator vane, in accordance with the spanwise subdivision of the vane into 11 strips. It is possible to observe the higher capability of particles to stick to the pressure side of the stator vane. The vane surface appears contaminated in a uniform way, and the deposits do not afflict a specific area. In general, the suction side shows a more irregular trend, especially close to the end wall regions.

The localization of the deposits on the blade represents a key aspect in the fouling phenomenon. In particular, the presence of the dangerous particles at the top of the blade could be responsible for a greater drop in compressor performance. As reported by Aldi et al. [28], the effects of fouling at the blade tip (e.g., the increase in surface roughness) have a greater influence on compressor performance degradation. The difference in the deposits between the pressure side and suction side is also important. As pointed out by Morini et al. in Ref. [29], the effects of fouling on the suction side (e.g., the increase in surface roughness) have a greater influence on compressor performance degradation.

Conclusions

In this paper, an extended numerical analysis of microparticle ingestion and adhesion in a transonic axial compressor stage is carried out. The NASA Stage 37 is considered the reference

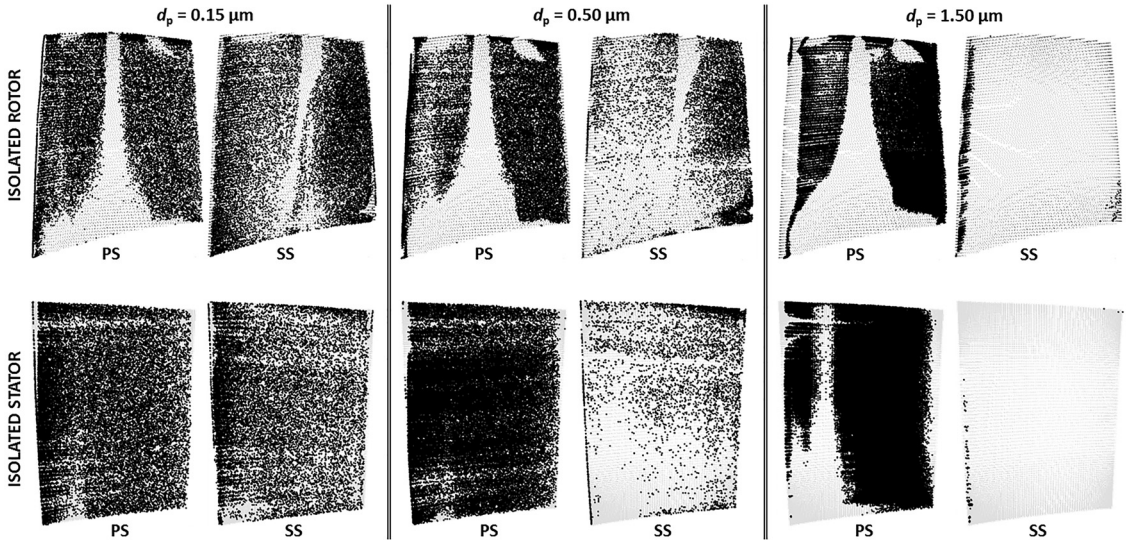

Fig. 10 Particle deposition patterns for the isolated rotor and stator

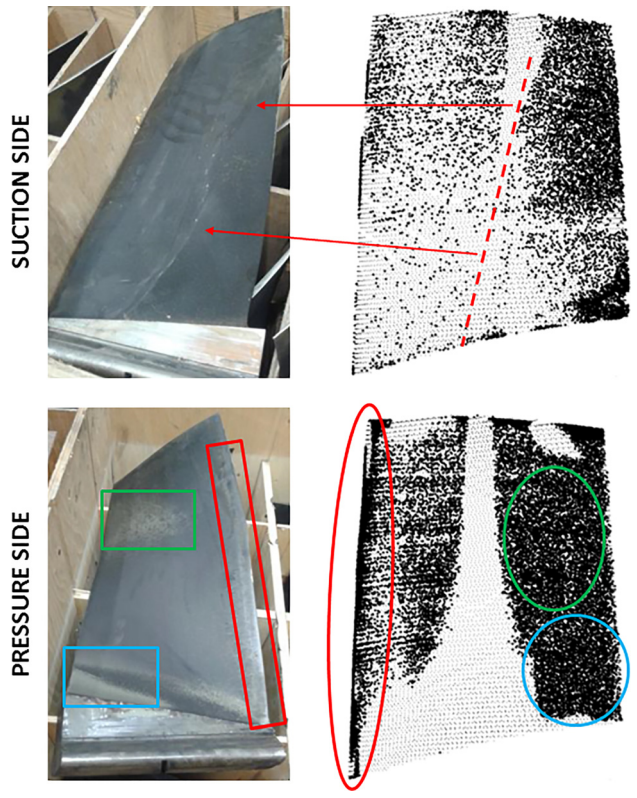

Fig. 11 Qualitative comparison between the actual deposits on the rotor blade [23] and numerical results

compressor stage. Numerical simulations are performed by using realistic field data for air contaminant concentration and filtration efficiency. Particle trajectories are predicted by means of an Eulerian–Lagrangian CFD approach, with separate particle injections for the isolated rotor and stator cascades. The location and the kinematic characteristics of particle impact on the blade surface are determined. These data are then used to calculate the sticking probability of particles that impact on the rotor blade and stator vane, defining the zones characterized by a high probability of particle deposition. A postprocess computational strategy is then used in order to consider the effect exerted by the rotor blade on the deposition zone location on the stator vane.

The key results obtained in this work can be summarized as follows: (i) the percentage of particles that hit the rotor blade and stator vane increases with the diameter of particles and, (ii) by increasing the particle diameter, the suction side is less affected by particle impacts than the pressure side. Regarding the kinematic characteristics of particle impact and its sticking probability, the following results are obtained: (i) the particle impact velocity depends on several factors (surface local curvature and fluid dynamic phenomena, such as flow separation and tip leakage vortex) and (ii) on the suction side, the smallest particles are the most numerous from a fouling point of view, due to the high total number of particles characterized by a sticking probability greater than 0.5. In general, the rotor blade and stator vane show almost the same behavior in relation to particle sticking. In fact, the suction side is less affected by deposits by increasing the particle diameter, and bigger particles stick only to the pressure side.

The understanding of fouling mechanisms in compressors is still a challenge for manufacturers and users. An increase in the knowledge of fouling through the use of numerical codes may therefore constitute a decisive element for better planning of turbomachinery maintenance.

Acknowledgment

The authors would like to thank Devid Dainese MSc for his valuable work in performing the particle postprocess.

Nomenclature

d = diameter
m = mass flow rate
St = Stokes number
U = averaged velocity
u_t = shear velocity
v = velocity
y^+ = non-dimensional distance

Greek Symbols

α = impact angle
β = total pressure ratio
η = efficiency
μ = dynamic viscosity
τ_w = wall shear stress
τ^+ = nondimensional particle relaxation time
ν = kinematic viscosity
ρ = density

Subscripts and superscripts

f = filtration system
h = hydraulic
hit = particle that impact a surface
i = impact
n = normal direction
p = particle
side = side (referring to the blade and vane side)

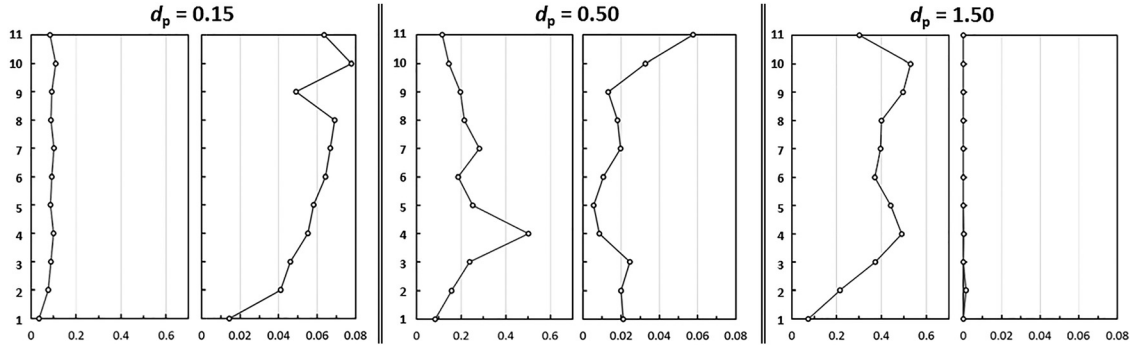

Fig. 12 Trends of the ratio $\eta_{hit,SP>0.5}$ for the coupled stator according to the spanwise subdivision of the stator vane

t = tangential direction
1 = inlet section of the stage
3 = outlet section of the stage

Acronyms

CFD = computational fluid dynamics
DRW = discrete random walk
PS = pressure side
SP = sticking probability
SS = suction side

Appendix A

Overall Impact Patterns

All the particle impact patterns are shown in Fig. 13. Each pattern represents the projection of the fouled airfoil into a perpendicular plane with respect to the spanwise direction. On the left side, the spanwise station and the correspondent percentage of the blade span are reported. The rotor blade and stator vane are divided by 11 strips along the spanwise direction and each dot

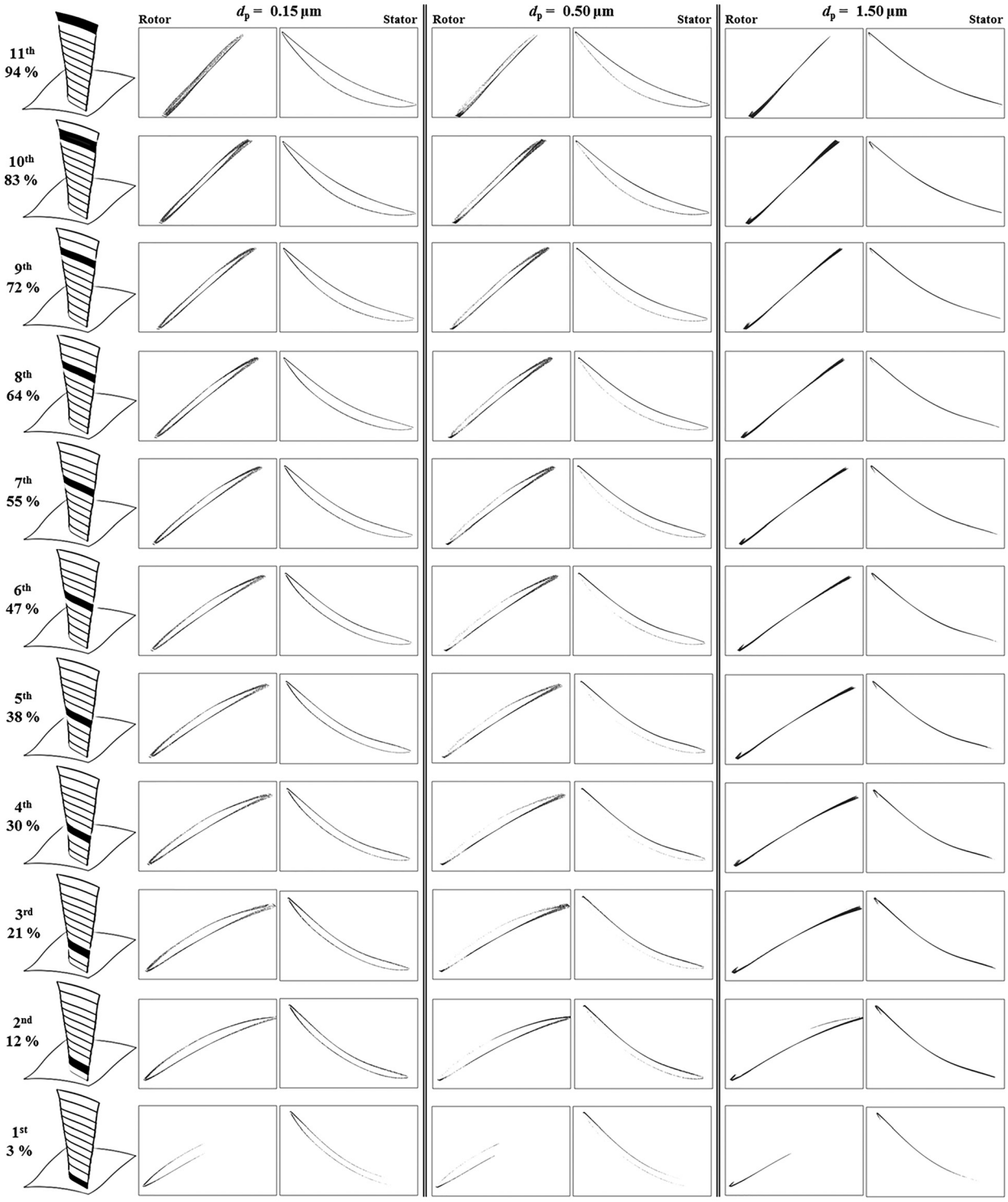

Fig. 13 Spanwise subdivision (left side) and overall impact patterns

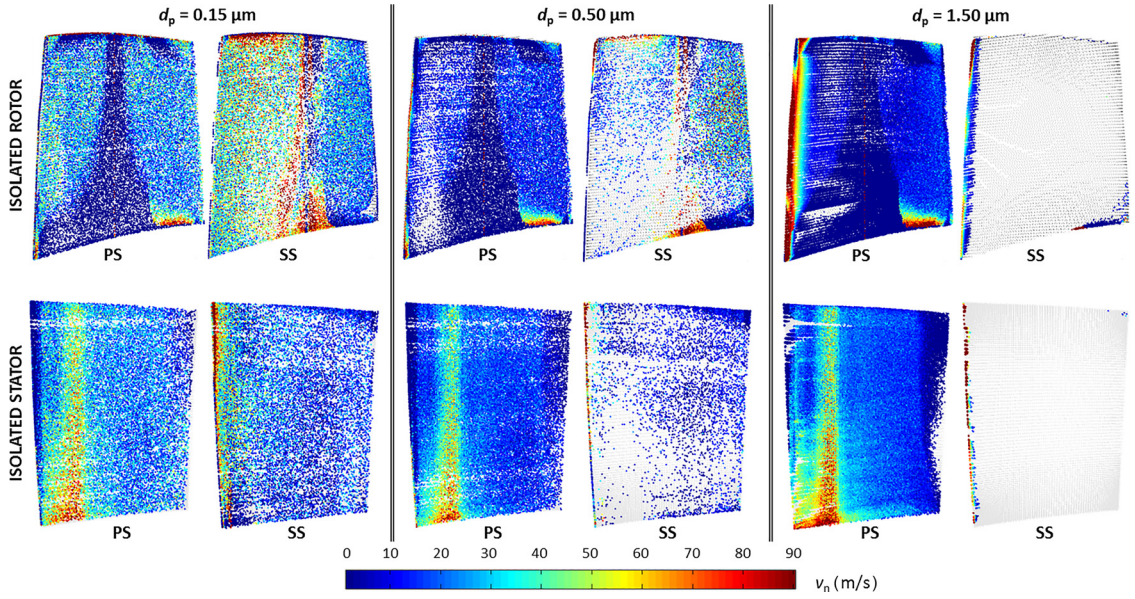

Fig. 14 Particle normal impact velocity for the isolated rotor and stator

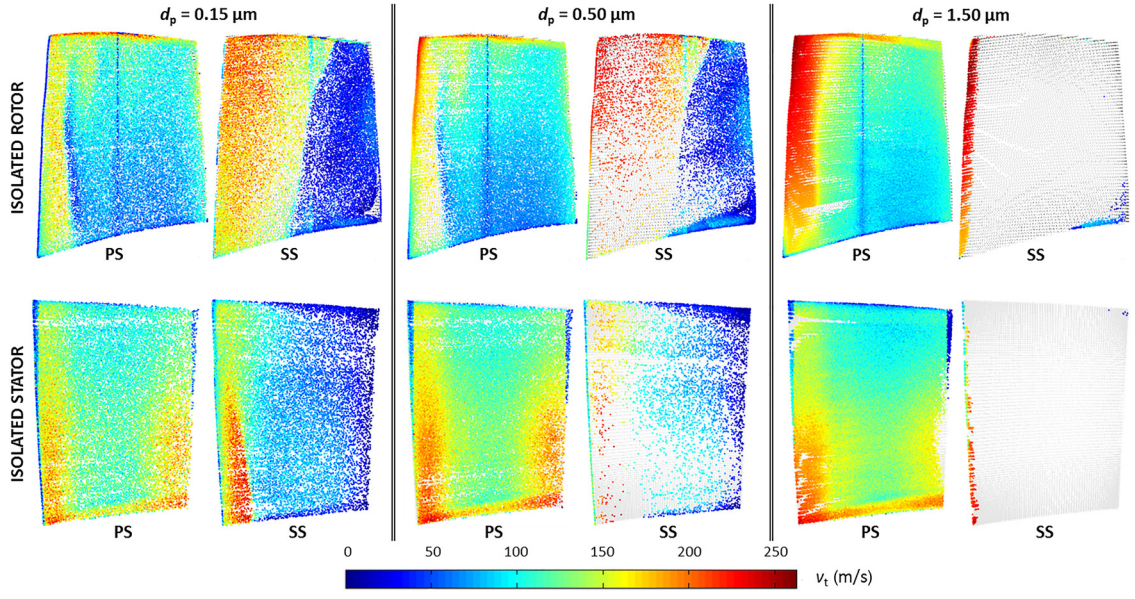

Fig. 15 Particle tangential impact velocity for the isolated rotor and stator

represents a single particle that hits the blade. Because of the shape of the hub, which develops along the streamwise direction with different diameters, the projection of the rotor blade is not complete, and only the first half of the airfoil can be represented.

Appendix B

Normal and Tangential Impact Velocity Components

The modules of the particle normal v_n and tangential v_t impact velocity components are reported in Figs. 14 and 15, respectively, for the rotor blade and the stator vane. Each dot is colored by the normal/tangential impact velocity and is superimposed with respect to the mesh node that provides the blade shape.

References

[1] Wilcox, M., Kurz, R., and Brun, K., 2011, "Successful Selection and Operation of Gas Turbine Inlet Filtration Systems," 40th Turbomachinery Symposium, Houston, TX, pp. 254–268.
[2] Kurz, R., and Brun, K., 2012, "Fouling Mechanism in Axial Compressors," ASME J. Eng. Gas. Turbine Power, **134**(3), p. 032401.
[3] Suman, A., Kurz, R., Aldi, N., Morini, M., Brun, K., Pinelli, M., and Spina, P. R., 2015, "Quantitative CFD Analyses of Particle Deposition on a Transonic Axial Compressor Blade, Part I: Particle Zones Impact," ASME J. Turbomach., **137**(2), p. 021009.
[4] Suman, A., Morini, M., Kurz, R., Aldi, N., Brun, K., Pinelli, M., and Spina, P. R., 2015, "Quantitative CFD Analyses of Particle Deposition on a Transonic Axial Compressor Blade, Part II: Impact Kinematics and Particle Sticking Analysis," ASME J. Turbomach., **137**(2), p. 021010.
[5] Carameros, A. H., 1956, "El Paso's Gas-Turbine Operating Experience," ASME Paper No. 56-GTP-6.
[6] Suman, A., Kurz, R., Aldi, N., Morini, M., Brun, K., Pinelli, M., and Spina, P. R., 2016, "Quantitative CFD Analyses of Particle Deposition on a Subsonic

Axial Compressor Blade," ASME J. Eng. Gas Turbine Power, **138**(1), p. 012603.

[7] Tarabrin, A. P., Schurovsky, V. A., Boldrov, A. I., and Stalder, J.-P., 1998, "Influence of Axial Compressor Fouling on Gas Turbine Unit Performance Based on Different Schemes and With Different Initial Parameters," ASME Paper No. 98-GT-416.

[8] Syverud, E., Brekke, O., and Bakken, L. E., 2005, "Axial Compressor Deterioration Caused by Saltwater Ingestion," J Turbomach, **129**(1), pp. 119–126.

[9] Zagnoli, D., Prenter, R., Ameri, A., and Bons, J. P., 2015, "Numerical Study of Deposition in a Full Turbine Stage Using Steady and Unsteady Methods," ASME Paper No. GT2015-43613.

[10] Suzuki, M., Inaba, K., and Yamamoto, M., 2008, "Numerical Simulation of Sand Erosion Phenomena in Rotor/Stator Interaction of Compressor," J. Therm. Sci., **17**(2), pp. 125–133.

[11] Ghenaiet, A., 2012, "Study of Sand Particle Trajectories and Erosion Into the First Compression Stage of a Turbofan," ASME J. Turbomach., **134**(5), p. 051025.

[12] Tabakoff, W., Hamed, A., and Metwally, M., 1991, "Effect of Particle Size Distribution on Particle Dynamics and Blade Erosion in Axial Flow Turbines," ASME J. Eng. Gas Turbine Power, **113**(4), pp. 607–615.

[13] Hamed, A. A., Tabakoff, W., Rivir, R. B., Das, K., and Arora, P., 2005, "Turbine Blade Surface Deterioration by Erosion," ASME J. Turbomach., **127**(3), pp. 445–452.

[14] Ghenaiet, A., 2014, "Study of Particle Ingestion Through Two-Stage Gas Turbine," ASME Paper No. GT2014-25759.

[15] Reid, L., and Moore, R. D., 1978, "Design and Overall Performance of Four Highly-Loaded, High-Speed Inlet Stages for an Advanced High-Pressure-Ratio Core Compressor," Technical Report, Report No. NASA TP 1337.

[16] ANSYS Fluent, 2013, "Release 15.0, User Manual," ANSYS, Canonsburg, PA.

[17] Ahlert, K., 1994, "Effects of Particle Impingement Angle and Surface Wetting on Solid Particle Erosion of AISI 1018 Steel," M.S. thesis, Department of Mechanical Engineering, The University of Tulsa, Tulsa, OK.

[18] Forder, A., Thew, M., and Harrison, D., 1998, "A Numerical Investigation of Solid Particle Erosion Experienced Within Oilfield Control Valves," Wear, **216**(2), pp. 184–193.

[19] Zohdi, T. I., 2004, "Modeling and Direct Simulation of Near-Field Granular Flows," Int. J. Solid Struct., **42**(■), pp. 539–564.

[20] Tian, T., and Ahmadi, G., 2006, "Particle Deposition in Turbulent Duct Flows—Comparisons of Different Model Predictions," J. Aerosol Sci., **38**(■), pp. 377–397.

[21] Gbadebo, S. A., Cumpsty, N. A., and Hynes, T. P., 2005, "Three-Dimensional Separations in Axial Compressors," ASME J. Turbomach., **127**(2), pp. 331–339.

[22] Poppe, T., Blum, J., and Henning, T., 2000, "Analogous Experiments on the Stickiness of Micron-Sized Preplanetary Dust," Astrophys. J., **533**(1), pp. 454–471.

[23] Silingardi, A., Astrua, P., Piola, S., and Ventrucci, I., 2013, "A Method for a Reliable Prediction of Heavy Duty Gas Turbines Performance Degradation due to Compressor Aging Employing Field Test Data," Power Gen Europe, June 4–6, Messe, Wien, Austria.

[24] Cumpsty, N. A., 1989, *Compressor Aerodynamics*, Longman Scientific & Technical, Harlow, UK.

[25] Suder, K. L., Chima, R. V., Strazisar, A. J., and Roberts, W. B., 1995, "The Effect of Adding Roughness and Thickness to a Transonic Axial Compressor Rotor," ASME J. Turbomach., **117**(4), pp. 491–505.

[26] Balan, C., and Tabakoff, W., 1984, "Axial Flow Compressor Performance Deterioration," 20th Joint Propulsion Conference, AIAA Meeting Paper, ■.

[27] Morini, M., Pinelli, M., Spina, P. R., and Venturini, M., 2010, "Computational Fluid Dynamics Simulation of Fouling on Axial Compressor Stages," ASME J. Eng. Gas Turbine Power, **132**(7), p. 072401.

[28] Aldi, N., Morini, M., Pinelli, M., Spina, P. R., Suman, A., and Venturini, M., 2014, "Performance Evaluation of Non-Uniformly Fouled Axial Compressor Stages by Means of Computational Fluid Dynamics Analyses," ASME J. Turbomach., **136**(■), p. 021016.

[29] Morini, M., Pinelli, M., Spina, P. R., and Venturini, M., 2011, "Numerical Analysis of the Effects of Non-Uniform Surface Roughness on Compressor Stage Performance," ASME J. Eng Gas Turbine Power, **133**(7), p. 072402.

AQ5 AQ6 AQ4